Deep-Learning-Assisted Dual-Mode Predictive Yaw Stability Control for Heavy Road Vehicles

Indra Mandal[1], Shravan S. Devadiga[2], Pavel Vijay Gaurkar[3], Mahesh Shridhare[4], Sriram Sivaram [5], and Shankar C. Subramanian[6]

***Abstract*— Heavy commercial road vehicles (HCRVs) can loss directional stability during combined steering and emergency braking (CSB) on low- and split-friction roads, where pneumatic brake delays and strong lateral–roll coupling limit corrective yaw-moment capacity. To bridge this safety gap, this paper proposes a lightweight, deep-learning (DL) -assisted reference yaw-rate generator by fusing a steady-state bicycle prior with a parameter-efficient neural residual trained on synthesized data from IPG TruckMaker® which can ensure runtime safety and out-of-distribution gating. The reference yaw rate is evaluated in closed loop as the tracking target of a dual-mode framework based nonlinear model predictive control (D-NMPC) based unified electronic stability control (ESC) system that realises corrective direct yaw moment through differential braking, by intelligently switching regimes: executing pressure overlays during non-braking phases and utilizing slip modification during active braking. This approach allows seamless coordination with an Optimal Reference Slip Algorithm (ORSA) and a three-phase previously developed ABS algorithm (SWATA). This is Evaluated on an IPG TruckMaker® pneumatic-brake hardware-in-the-loop (HiL) platform. Compared to an ABS-only baseline, the proposed ESC robustly bounds sideslip and lateral load transfer ratio margins, delivering a 30–40% improvement in yaw tracking and directional stability during critical medium friction-road maneuvers.**

***Keywords*—Electronic stability control, neural residual model, nonlinear model predictive control, roll–yaw control, reference yaw-rate generation.**

I. Introduction

A. Motivation

Road traffic injuries remain a major public-health concern, with HCRVs contributing a disproportionate share of severe outcomes despite representing a smaller fraction of the vehicle fleet [1], [2]. From a vehicle-dynamics perspective, HCRVs are challenging platforms for ESC because yaw stability and roll stability are coupled through load transfer, the center-of-gravity height varies substantially with payload, and the available corrective dynamic yaw moment is often limited by brake actuator bandwidth [3]–[5]. These limitations are amplified in CSB on low- and split-friction pavements, where ABS can preserve wheel slip but may still permit excessive yaw response and sideslip angle growth that degrades directional performance [5].

B. Related Work

CSB maneuvers induce severe directional and roll instabilities, further complicated by substantial load transfer and pneumatic actuation delays [4], [5]. Consequently, recent research integrates wheel slip regulation with DYC to actively manage these heavy-vehicle-specific actuator limits during critical interventions [6], [7]. NMPC effectively handles these multi-objective requirements and operational constraints [8], [9]. Simultaneously, hybrid physics-informed neural networks demonstrate superior accuracy in capturing highly nonlinear lateral vehicle dynamics [10], [11]. Evaluating these control architectures requires HiL testing, as physical pneumatic pressure regulation strictly limits the achievable transient yaw response [12], [13].

C. Research Gap

Existing HCRV stability literature predominantly uses simplified, physics-based reference models with conventional sliding-mode control (Table I). This reveals a few critical research gaps for vehicles operating under the variable surface.

First, while hybrid networks improve lateral dynamics prediction [10], their empirical evaluation as real-time, parameter-efficient reference yaw-rate generators for HCRVs under severe lateral-roll coupling remains unexplored.

Second, there is a distinct lack of this dual-mode framework and integrated architectures combining DL-assisted reference generation with a constrained D-NMPC framework, evaluated within a pneumatic-brake HiL setup.

D. Contributions

To address the identified gaps, this paper presents three interconnected contributions for HCRV stability control. First, it proposes a DL-assisted reference yaw-rate generator that uses a parameter-efficient neural residual relying solely on steering angle and longitudinal speed. Second, this reference is tracked by a roll-aware D-NMPC that explicitly manages pneumatic actuator saturation and lateral load transfer constraints. Finally, the complete architecture is evaluated on an IPG TruckMaker® HiL platform, demonstrating the

*The authors thank the Madras Engineering Industries Private Limited, Chennai, India, for their support of this research through the grant RB21221488EDMADA008265. The authors also acknowledge the funding provided by the Ministry of Skill Development and Entrepreneurship, Government of India, through the grant EDD/14-15/023/MOLE/NILE.

[1]Research Scholar, Department of Engineering Design, Indian Institute of Technology Madras, Chennai, India. ed24s014@smail.iitm.ac.in

[2]Research Scholar, Department of Engineering Design, Indian Institute of Technology Madras, Chennai, India. ed22d402@smail.iitm.ac.in

[3]Lead Engineer, Controls Division, Madras Engineering Industries Private Ltd., Chennai, India. pavelgaurkar@gmail.com

[4]Madras Engineering Industries Private Ltd., Chennai, India. shridhare@mei.co.in

[5]Madras Engineering Industries Private Ltd., Chennai, India. ssivaram@mei.co.in

[6]Professor, Department of Engineering Design, Indian Institute of Technology Madras, Chennai, India. shankarram@iitm.ac.in

TABLE I: Literature survey on yaw stability and ESC strategies for heavy vehicles

S.R. No.	Author(s)	Variable Required[1]	Control Method[2]		Reference Model (DYC)[3]	Vehicle Type[4]	Tire Model for Control Design	HiL / VT[5]
			ABS	DYC				
1	Mirzaeinejad & Mirzaei (2014) [14]	$\dot{\psi}, \lambda$	Nonlinear ABS	Implicit DYC via Torque Opt.	Nonlinear Single-Corner Model	PC	Magic Formula	No
2	Morrison & Cebon (2017) [4]	$\dot{\psi}, \beta, \psi_{12}, \lambda$	SMC	RBA	SS, lateral dyn. with roll coupling	HCRV	Fancher tire model	No
3	Wang et al. (2018) [6]	$\dot{\psi}, \beta, \lambda$	SMC	SMC	SS, 2-DoF bicycle Model	PC	Magic Formula	VT
4	Li et al. (2019) [15]	$\dot{\psi}, \beta, \lambda$	SMC	PID	2 DoF model for three-axle vehicle	HCRV	Dugoff tire model	HiL
5	Patil et al. (2022) [5]	$\dot{\psi}, \lambda$	SMC	SMC	SS, 3-DoF Lateral dyn. with roll coupling	HCRV	Magic Formula 6.1	HiL
6	**Proposed Work**	$\boldsymbol{\dot{\psi}, \beta, \lambda}$, **LTR**	**ORSA-Adapted SWATA ABS**	**D-NMPC**	**Bicycle Model + Deep Residual NN**	**HCRV**	**Pacejka (Truck, Comb. Slip)**	**HiL**

Notes: [1]$\dot{\psi}$: yaw rate; β: sideslip; ψ_{12}: art. yaw rate; λ: wheel slip. [2]ABS: anti-lock braking; DYC: direct yaw-moment control; SMC: sliding mode; RBA: rule-based. [3]SS: steady-state; DoF: degree of freedom. [4]PC: passenger car; HCRV: heavy commercial road vehicle. [5]HiL: hardware-in-the-loop; VT: vehicle testing.

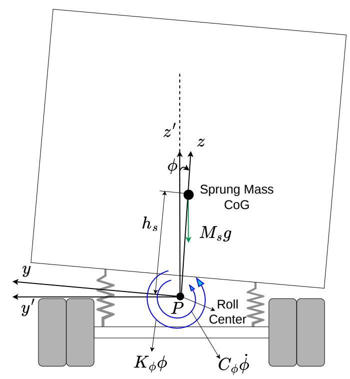

Fig. 1: Free-body diagram of the HCRV in roll plane.

integration of the DL-based reference and D-NMPC with an ORSA and SWATA ABS under realistic pneumatic delays.

II. Vehicle Modeling and Experimental Platform

A. Vehicle Configuration and Assumptions

The target vehicle is a rigid, single-unit 4×2 HCRV. To formulate a computationally efficient control-oriented prediction model, the following standard assumptions are applied [5]: 1) pitch dynamics are neglected, allowing longitudinal load transfer to be treated quasi-statically; 2) steering angles are assumed small; and 3) the sprung mass rolls about a fixed horizontal ground-parallel axis.

B. Lateral, Yaw, and Roll Dynamics

Using a body-fixed frame, the non-linear 3-Degrees of Freedom chassis dynamics capturing the vehicle's lateral velocity, $v_y(t)$, yaw rate, $r(t)$, and roll angle, $\phi(t)$, are established. The associated governing differential equations, which balance the inertial forces and moments with the lateral tire forces, corrective direct yaw moment, and suspension roll characteristics, have been comprehensively formulated and experimentally evaluated in previous studies [5].

The vehicle sideslip angle is $\beta(t) = \tan^{-1}(v_y(t)/v_x(t))$, and the respective axle slip angles are derived using standard kinematic relations [5].

C. Normal Loads and Rollover Indicator

To retain critical pitch and lateral load transfer effects without expanding the differential state vector, the instantaneous wheel normal loads, $F_{z,ij}(t)$, are computed algebraically from the longitudinal and lateral accelerations, as formulated in [5]. The rollover propensity is actively monitored via the lateral Load Transfer Ratio:

$$\mathrm{LTR}(t) = \frac{\big(F_{z,\mathrm{fr}}(t) + F_{z,\mathrm{rr}}(t)\big) - \big(F_{z,\mathrm{fl}}(t) + F_{z,\mathrm{rl}}(t)\big)}{\sum_{ij} F_{z,ij}(t)}. \quad (1)$$

A conservative intervention band limits the operational state, triggering rollover-preventive action when $|\mathrm{LTR}(t)| \geq 0.8$ and releasing it when $|\mathrm{LTR}(t)| \leq 0.7$. These specific activation and hysteresis thresholds are adopted from established heavy vehicle stability research to guarantee timely intervention prior to irreversible wheel lift-off while simultaneously mitigating detrimental control chattering [16].

D. Tire Model and Pneumatic Brake Actuation

The HiL plant employs a combined-slip Magic Formula tire model [17] within IPG TruckMaker®. The braking slip ratio $\lambda_{ij}(t)$ is defined conventionally as the normalized difference between the wheel-center longitudinal speed and the tire's tangential speed [5].

To capture the essential physical delays that limit control bandwidth, each electro-pneumatic regulator is modeled as a first-order system, as experimentally evaluated in [5], [18].

III. ESC–ABS Architecture and HiL Platform

Figure 2 illustrates the proposed integrated control architecture, which systematically coordinates reference generation, predictive yaw stabilization, and physical wheel-slip regulation. An estimator first estimates longitudinal speed $v_x(t)$, sideslip angle $\beta(t)$, and wheel-slip ratios $\lambda_{ij}(t)$ using filtered sensor data. These states feed the DL generator to produce a bounded yaw-rate target $r_{\mathrm{ref}}(t)$ and the ORSA to determine the friction-adaptive optimal slip $\lambda_{\mathrm{opt}}(t)$ [13]. Tracking these targets, the D-NMPC computes a corrective direct yaw moment while explicitly managing pneumatic actuator constraints. To ensure compatibility with active braking, the D-NMPC dynamically switches its differential braking execution from direct pressure overlays during pure cornering to slip-target shaping during CSB maneuvers. A supervisory command blender resolves these stability interventions with driver demands, passing the final targets to a three-phase SWATA ABS [19]. The complete framework is evaluated on a HiL platform that couples IPG TruckMaker® and MATLAB/Simulink® with physical electro-pneumatic brake hardware, subjecting commanded pressures $P_{\mathrm{des},ij}(t)$ to actual pneumatic delays before realization as wheel torque.

IV. DL-Assisted Reference Yaw-Rate Generator

HCRVs operating on variable-friction surfaces experience severe lateral–roll coupling during CSB maneuvers that standard bicycle models inherently fail to capture. To establish an accurate yet interpretable yaw-rate reference, this paper proposes a hybrid framework that augments a steady-state prior with a parameter-efficient neural residual. While the bicycle model provides a baseline, the neural residual explicitly

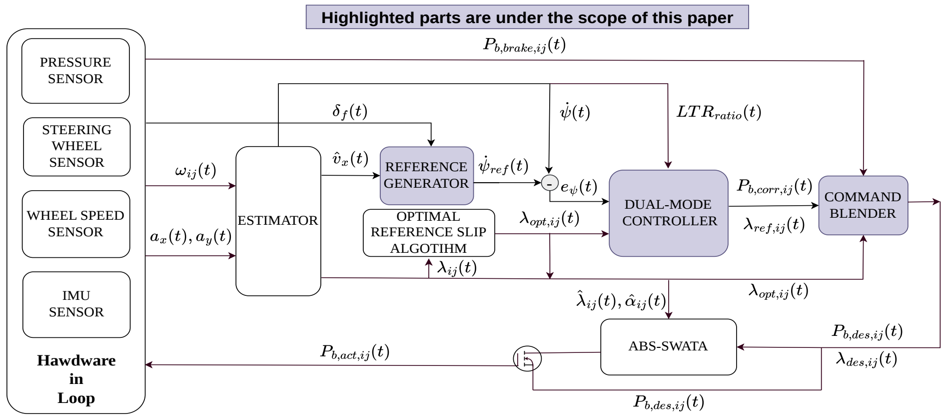

Fig. 2: Proposed integrated control architecture combining DL-assisted reference generation, D-NMPC, and ABS.

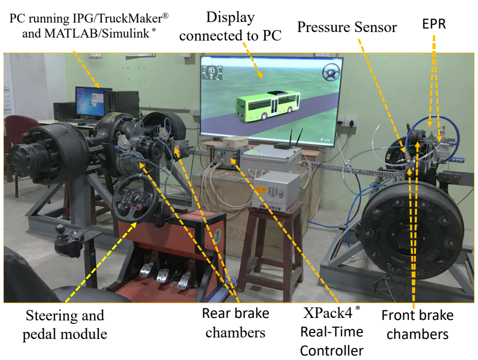

Fig. 3: HiL platform coupling IPG TruckMaker® vehicle dynamics with physical pneumatic brake hardware.

captures the complex yaw–roll dynamics and tire saturation effects learned directly from high-fidelity TruckMaker® data, combined explicit runtime safety guards.

A. Bicycle Prior and Hybrid Reference Definition

Let $\delta_{\text{road}}(t)$ denote the effective front-axle road-wheel steering angle (after steering-system mapping), $v_x(t)$ the longitudinal speed, and L the wheelbase. The neutral-steer yaw-rate prior is

$$r_0(t) = \frac{v_x(t)}{L}\,\delta_{\text{road}}(t). \tag{2}$$

The DL-assisted reference yaw rate is defined as

$$r_{\text{ref}}(t) = r_0(t) + \bar{r}_\Delta(t), \tag{3}$$

where $\bar{r}_\Delta(t)$ is a bounded, filtered residual correction produced by the neural residual block and the runtime safety guards detailed in Section IV-C.

B. Residual Network, Filtering, and Normalisation

The residual uses only the measured pair $\big(v_x(t), \delta_{\text{road}}(t)\big)$ to avoid parameter-heavy dependence on uncertain tire and load states. Using training-set statistics $\boldsymbol{\mu}_{\text{s}}$ and $\boldsymbol{\sigma}_{\text{s}}$, the normalised feature vector $\hat{\mathbf{s}}(t)$ is computed element-wise as

$$\hat{\mathbf{s}}(t) = \frac{\mathbf{s}(t) - \boldsymbol{\mu}_{\text{s}}}{\boldsymbol{\sigma}_{\text{s}}}. \tag{4}$$

A 2-hidden-layer (16–16) structure was selected by validation-based architecture screening under a parameter-budget constraint, which showed no consistent improvement from larger networks. A hyperbolic tangent activation was chosen for its smooth, bounded, signed nonlinearity, which is appropriate for residual yaw-rate correction:

$$\mathbf{h}^{(1)}(t) = \tanh\Big(\mathbf{W}^{(1)}\hat{\mathbf{s}}(t) + \mathbf{b}^{(1)}\Big), \tag{5}$$

$$\mathbf{h}^{(2)}(t) = \tanh\Big(\mathbf{W}^{(2)}\mathbf{h}^{(1)}(t) + \mathbf{b}^{(2)}\Big), \tag{6}$$

$$\Delta r_{\boldsymbol{\theta}}\big(\hat{\mathbf{s}}(t)\big) = \mathbf{W}^{(3)}\mathbf{h}^{(2)}(t) + b^{(3)}. \tag{7}$$

Here, $\mathbf{W}^{(1)}$ and $\mathbf{W}^{(2)}$ are the hidden layer weight matrices, $\mathbf{W}^{(3)}$ is the output weight vector, $\mathbf{h}^{(1)}$ and $\mathbf{h}^{(2)}$ are the hidden state vectors, $\mathbf{b}^{(1)}$ and $\mathbf{b}^{(2)}$ are bias vectors, and $b^{(3)}$ is the scalar output bias.

C. Runtime Safety Guards

To ensure conservative operation when the operating point is weakly represented by the training distribution, an out-of-distribution distance is computed from the normalised inputs $\hat{\mathbf{s}}(t) = \big[x_1(t) \;\; x_2(t)\big]^\top$:

$$d(t) = \max\Big(\big|x_1(t)\big|,\; \big|x_2(t)\big|\Big). \tag{8}$$

Let z_{soft} and z_{hard} denote soft and hard thresholds derived from training percentiles. The blending factor is

$$\alpha(t) = \begin{cases} 1, & d(t) \le z_{\text{soft}}, \\ \dfrac{z_{\text{hard}} - d(t)}{z_{\text{hard}} - z_{\text{soft}}}, & z_{\text{soft}} < d(t) < z_{\text{hard}}, \\ 0, & d(t) \ge z_{\text{hard}}. \end{cases} \tag{9}$$

Thus the gated instantaneous residual is

$$\Delta r_{\text{inst}}(t) = \alpha(t)\,\Delta r_{\boldsymbol{\theta}}\big(\hat{\mathbf{s}}(t)\big). \tag{10}$$

For discrete-time implementation at sampling instants $t_k = kT_{\text{s}}$, a first-order residual low-pass filter is applied. Then the filtered residual is bounded as

$$\big|\bar{r}_\Delta(t_k)\big| \le r_{\text{clip}}, \tag{11}$$

and the final output is rate-limited to remain compatible with pneumatic pressure dynamics:

$$\big|r_{\text{ref}}(t_k) - r_{\text{ref}}(t_{k-1})\big| \le \dot{r}_{\max}\,T_{\text{s}}. \tag{12}$$

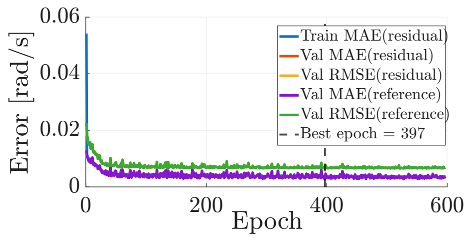

Fig. 4: Residual-network learning behaviour used to evaluate offline accuracy before HiL evaluation.

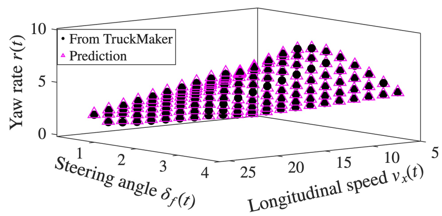

(a) TruckMaker® vs. predicted yaw rate $r(t)$.

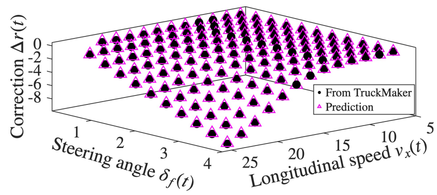

(b) TruckMaker® vs. predicted residual correction.

Fig. 5: TruckMaker® data vs. DL predictions for yaw rate and residual correction across varying δ_{road} and v_x.

D. Dataset Construction and Training Objective

The residual label is constructed from synthesised data of yaw-rate $r(t)$ taken from IPG TruckMaker® as

$$\Delta r^\star(t) = r(t) - r_0(t), \tag{13}$$

using manoeuvres spanning ramp-steer, sine-with-dwell, and CSB over multiple friction levels and speeds.

After preprocessing, the supervised dataset used for training contained $N_{\text{train}} = 17{,}070$ samples (with a held-out validation set of $N_{\text{val}} = 5{,}690$ samples and test set of $N_{\text{test}} = 1{,}980$ samples), with early stopping based on validation loss.

The network parameters $\boldsymbol{\theta}$ are learned offline by minimising a regularised Huber objective:

$$\mathcal{L}(\boldsymbol{\theta}) = \frac{1}{N_{\text{train}}} \sum_{k=1}^{N_{\text{train}}} \rho_\delta\Big(\Delta r_{\boldsymbol{\theta}}\big(\hat{\mathbf{s}}(t_k)\big) - \Delta r^\star(t_k)\Big) + \lambda_{\text{reg}} \|\boldsymbol{\theta}\|_2^2, \tag{14}$$

where λ_{reg} is the ℓ_2 regularisation weight and

$$\rho_\delta(e) = \begin{cases} \frac{1}{2}e^2, & |e| \le \delta, \\ \delta|e| - \frac{1}{2}\delta^2, & |e| > \delta. \end{cases} \tag{15}$$

V. Dual-Mode Framework Based Nonlinear Model Predictive Electronic Stability Control

The primary rationale for employing a NMPC framework is its inherent capability to systematically optimize dynamic reference tracking while actively anticipating and enforcing strict operational constraints. For HCRVs, generating a corrective direct yaw moment $M_z(t)$ to track the target $r_{\text{ref}}(t)$ requires simultaneous management of strongly coupled yaw–roll dynamics, pneumatic actuator saturation, and absolute boundaries on sideslip and lateral load transfer. Concurrently, the D-NMPC layer solves for the required differential braking interventions, computing an optimal yaw moment that enforces directional stability without violating the critical rollover or sideslip thresholds.

A. Prediction Model

The D-NMPC uses the continuous-time state vector

$$\boldsymbol{x}(t) = \begin{bmatrix} v_y(t) & r(t) & \phi(t) & \dot{\phi}(t) \end{bmatrix}^\top, \tag{16}$$

where $v_y(t)$ is lateral velocity, $r(t)$ is yaw rate, and $\phi(t)$ and $\dot{\phi}(t)$ are sprung-mass roll angle and roll rate. The longitudinal speed $v_x(t)$ is treated as a measured scheduling signal and a normalised control input $u_{\text{s}}(t) \in [-1, 1]$ mapped to yaw moment as

$$M_z(t) = k_{M_z}\, u_{\text{s}}(t), \tag{17}$$

where $k_{M_z} > 0$ is selected from achievable differential-braking capacity.

Let $\boldsymbol{\xi}(t)$ collect measured scheduling variables, including $v_x(t)$ and $\delta_{\text{road}}(t)$, and any stiffness estimates used by the reduced model. The prediction dynamics are written compactly as

$$\dot{\boldsymbol{x}}(t) = f\Big(\boldsymbol{x}(t), u_{\text{s}}(t), \boldsymbol{\xi}(t)\Big), \tag{18}$$

where $f(\cdot)$ implements the lateral–yaw–roll model of Section II, including slip-angle computation, and load transfer.

B. Nonlinear Model Predictive Control Problem

Over a horizon of N steps, the optimiser computes $\mathbf{U} = \{u_0, \dots, u_{N-1}\}$ and slack variables $\mathbf{S} = \{s_{\beta,k}, s_{L,k}\}_{k=0}^{N-1}$ by solving

$$\begin{aligned} \min_{\mathbf{U},\mathbf{S}} \quad & J(\mathbf{X}, \mathbf{U}, \mathbf{S}) \qquad\qquad (19)\\ \text{s.t.} \quad & \boldsymbol{x}_{k+1} = f_{\text{d}}(\boldsymbol{x}_k, u_k, \boldsymbol{\xi}_k), \quad k = 0, \dots, N-1, \\ & u_{\min} \le u_k \le u_{\max}, \quad k = 0, \dots, N-1, \\ & -\beta_{\max} - s_{\beta,k} \le \beta(t_k) \le \beta_{\max} + s_{\beta,k}, \\ & -\mathrm{LTR}_{\max} - s_{L,k} \le \mathrm{LTR}(t_k) \le \mathrm{LTR}_{\max} + s_{L,k}, \\ & s_{\beta,k} \ge 0, \quad s_{L,k} \ge 0, \quad k = 0, \dots, N-1, \end{aligned}$$

where $\beta(t_k)$ and $\mathrm{LTR}(t_k)$ are computed using Section II. The bounds $\beta_{\max}$ and $\mathrm{LTR}_{\max}$ enforce directional stability and rollover margin, while the slacks ensure feasibility under severe transients and actuator limits.

C. Cost Function for Safety Constrained Reference Tracking

Let $r_{\text{ref}}(t_k)$ be the DL-assisted reference from (3), and let $\beta_{\text{ref}}(t_k)$ denote the sideslip reference. The stage cost is

$$\begin{aligned} \ell(t_k) = {} & q_r\big(r(t_k) - r_{\text{ref}}(t_k)\big)^2 + q_\beta\big(\beta(t_k) - \beta_{\text{ref}}(t_k)\big)^2 \\ & + q_\phi\, \phi(t_k)^2 + q_{\dot{\phi}}\, \dot{\phi}(t_k)^2 + r_u\, u_k^2 + s_u\big(u_k - u_{k-1}\big)^2 \\ & + \rho_\beta\, s_{\beta,k}^2 + \rho_L\, s_{L,k}^2, \end{aligned} \tag{20}$$

and the total horizon cost is

$$J(\mathbf{X}, \mathbf{U}, \mathbf{S}) = \sum_{k=0}^{N-1} \ell(t_k) + \ell(t_N). \tag{21}$$

In (20), q_r penalises yaw-rate tracking error relative to the learned reference; q_β penalises sideslip deviation; q_ϕ and $q_{\dot\phi}$ penalise roll motion; r_u penalises yaw-moment effort; s_u penalises yaw-moment rate change for brake smoothness; and ρ_β and ρ_L penalise violations of the sideslip and lateral load transfer ratio constraints.

D. Dual-Mode Realisation of the Yaw-Moment Command

The optimiser outputs $M_z(t)$ through (17), but its realisation must remain compatible with wheel-slip regulation. Accordingly, two regimes are used:

1) Low-Braking Regime: Incremental Pressure Overlay: When driver braking is low and ABS intervention is inactive, the desired yaw moment is realised by a bounded incremental pressure overlay $\Delta P_{\mathrm{b},ij}(t)$ on selected wheels. The commanded pressure is enforced to be non-decreasing relative to the driver request:

$$P_{\mathrm{b,cmd},ij}(t) = \max\Big(P_{\mathrm{b,drv}}(t),\, P_{\mathrm{b,drv}}(t) + \Delta P_{\mathrm{b},ij}(t)\Big), \quad (22)$$

where the wheel-selection sign pattern for $\Delta P_{\mathrm{b},ij}(t)$ is chosen to generate the required yaw moment using differential braking.

2) Braking Regime: Slip-Target Shaping Around the Friction-Optimal Slip: When braking is significant, direct pressure overlays can conflict with wheel-slip regulation. In this regime, the yaw-moment request is mapped to per-wheel desired slips $\lambda_{\mathrm{des},ij}(t)$ around the optimal slip $\lambda_{\mathrm{opt}}(t)$:

$$\lambda_{\mathrm{des},ij}(t) = \max\Big(0, (\lambda_{\mathrm{opt}}(t) + \Delta\lambda_{ij}(t))\Big), \quad (23)$$

where $\Delta\lambda_{ij}(t)$ encodes the stabilising left–right slip differential consistent with the sign of $M_z(t)$ and the steering direction, and λ_{ub} is an upper bound for slip tracking.

The ABS then modulates the pressure to track $\lambda_{\mathrm{des},ij}(t)$:

$$P_{\mathrm{b,cmd},ij}(t) = \mathrm{SWATA}\Big(P_{\mathrm{b,drv}}(t),\, \lambda_{\mathrm{des},ij}(t)\Big), \quad (24)$$

where $\mathrm{SWATA}(\cdot)$ denotes the Slip- and Wheel-Acceleration-Threshold ABS algorithm with dynamic slip-target capability as described in [19].

VI. HiL Experiments and Results

This section reports the HiL evaluation of the proposed reference-yaw generation and dual-mode ESC–ABS architecture on a 4×2 HCRV with pneumatic brakes.

A. Test Matrix and Baselines

To robustly evaluate the coupled lateral–yaw–roll dynamics near the friction limit ($\mu = 0.5$), the testing matrix employs a standard Double Lane Change (DLC) and a J-turn maneuver. The J-turn trajectory strictly conforms to the U.S. FMVSS No. 136 testing protocol for heavy vehicle electronic stability control [20]. A constant steering input is used in all experiments to avoid driver adaptation. The following controller configurations are compared:

Open-loop (OL): ESC and ABS disabled.

ABS-only: Only ORSA + SWATA ABS active.

Proposed D-NMPC ESC: D-NMPC ESC tracking the DL-assisted reference yaw rate $r_{\mathrm{ref}}(t)$; in non-braking it applies pressure overlays, and in braking it shapes wheel-slip targets around ORSA.

B. Results: Double Lane Change

In Fig. 7(a)-(c), the open-loop truck suffers a severe loss of directional and roll stability during the high-speed DLC, characterized by divergent yaw rates, LTR saturation, and excessive roll angles. Conversely, the proposed D-NMPC ESC utilizes differential braking to induce a corrective yaw moment. This actively enforces tight $r_{\mathrm{ref}}(t)$ tracking and reliably confines both the LTR and roll dynamics within safe, recoverable margins throughout the maneuver.

C. Results: Braking-and-Cornering with ESC–ABS Coordination

The CSB case (Fig. 8) stresses HCRV stability because the brake-induced longitudinal slip reduces lateral force capacity while pneumatic delays limit fast yaw-moment build-up. After the marked braking onset, open-loop operation understeers and the vehicle departs the road (Fig. 8(a)) with a pronounced yaw-rate drop (Fig. 8(b)). ABS-only maintains

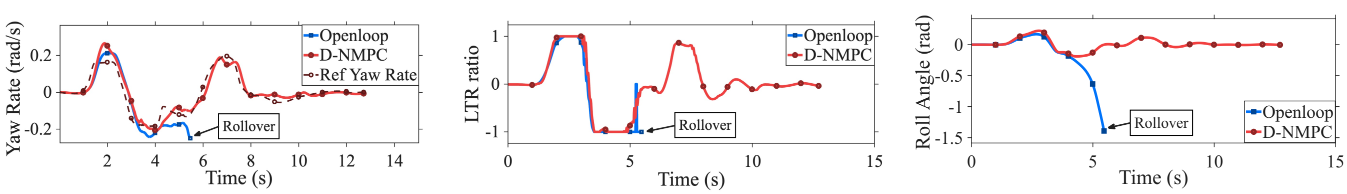

(a) Yaw rate ($\dot\psi$) tracking. (b) LTR ratio (LTR_{ratio}). (c) Roll angle $\dot\phi$.

Fig. 7: Double lane change, $\mu = 0.5$, $v_x(0) = 85$ km/h: stability using differential braking and reference-yaw tracking.

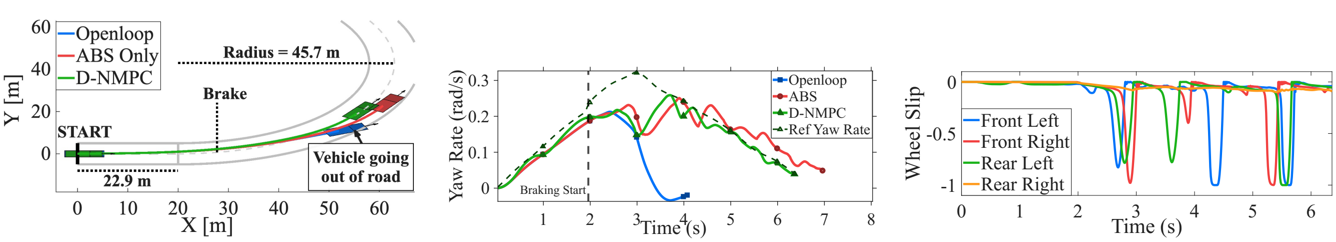

(a) X–Y trajectory. (b) Yaw rate $r(t)$ vs. $r_{\mathrm{ref}}(t)$. (c) NMPC slip shaping (braking mode).

Fig. 8: Braking-and-cornering HiL results: ABS-only vs. proposed D-NMPC, highlighting yaw tracking and slip shaping.

TABLE II: Summary of ESC performance metrics.

Sr. No.	Loading condition	Road friction coefficient μ	Initial speed (km/h)	Radius of curvatur (m)	Maneuver	Algorithm	Performance metrics						
							Braking distance (m)	Max sideslip angle (deg)	YTI (deg/s)	MNAE (%)	Max roll angle (deg)	Max LTR	Air Consumed (L)
1	Laden (16200 kg)	0.5	65	100	Only Cornering	Open-loop†	N/A	N/A	N/A	N/A	N/A	N/A	N/A
2						**D-NMPC**	N/A	**1.15**	**0.83**	**18.44**	**3.02**	**0.44**	**10**
3	Laden (16200 kg)	0.5	52	45.7	Braking + cornering	Open-loop†	N/A	N/A	N/A	N/A	N/A	N/A	N/A
4						ABS	40.15	6.76	3.07	56.31	3.58	0.49	50
5						**D-NMPC**	**34.75**	**5.59**	**2.39**	**54.02**	**3.01**	**0.41**	**50**
6	Laden (16200 kg)	0.5	65	100	Braking + cornering	Open-loop†	N/A	N/A	N/A	N/A	N/A	N/A	N/A
7						ABS	56.76	7.56	1.22	62.94	2.59	0.42	60
8						**D-NMPC**	**54.23**	**6.28**	**1.12**	**55.27**	**2.40**	**0.38**	**60**
9	Laden (16200 kg)	0.5	70	100	Braking + cornering	Open-loop†	N/A	N/A	N/A	N/A	N/A	N/A	N/A
10						ABS†	N/A	N/A	N/A	N/A	N/A	N/A	N/A
11						**D-NMPC**	**60.75**	**5.77**	**1.06**	**96.29**	**2.78**	**0.44**	**60**

Abbreviations & Metrics: N/A – not applicable. † Vehicle departed road. **YTI:** $\mathrm{YTI} = \frac{1}{T_2 - T_1} \int_{T_1}^{T_2} |r(t) - r_{\mathrm{ref}}(t)| \, \mathrm{d}t$, where $r(t)$ and $r_{\mathrm{ref}}(t)$ are measured and reference yaw rates over window $[T_1, T_2]$. **MNAE:** $\mathrm{MNAE} = \max_{t \in [T_1, T_2]} \frac{|r(t) - r_{\mathrm{ref}}(t)|}{\max(|r_{\mathrm{ref}}(t)|, \epsilon)} \times 100$ [%].

wheel rotation but exhibits larger yaw excursions around the reference, whereas the proposed D-NMPC maintains tighter yaw-rate tracking while staying in road center-line and a smaller sideslip envelope.

D. Quantitative Performance Evaluation

Table II gives the dynamic benefits of the proposed framework. The D-NMPC shortens the stopping distance by 5.4 m and lowers the peak sideslip by 17.3% compared to the ABS-only baseline during the FMVSS-aligned 52 km/h combined maneuver ($R = 45.7$ m). At 65 km/h ($R = 100$ m), it cuts the braking distance by 2.53 m and reduces the sideslip by 16.9%. Most importantly, the ABS-only car physically leaves the track when it enters at a speed of 70 km/h. In direct contrast, the D-NMPC maintains full directional and roll stability (with a peak LTR of only 0.44) and safely completes the maneuver. Additionally, these simultaneous improvements in yaw tracking and deceleration are made efficiently, without going over the baseline pneumatic air consumption in any test case.

VII. Conclusion

This paper presented a DL-assisted reference yaw-rate generator and a dual-mode ESC framework for HCRVs with pneumatic brakes, evaluated in TruckMaker® HiL. The safeguarded residual-learning reference provides a bounded target yaw response across steering and speed, enabling the D-NMPC to enforce directional stability objectives while respecting sideslip and rollover margins. HiL results on low-μ constant-radius maneuvers show that the proposed D-NMPC improves yaw-tracking consistency and reduces sideslip excursions relative to ABS-only operation, while preserving competitive braking distances. While HiL simulations validate real-time capability, future work will systematically quantify the computational load upon deployment in a real vehicle.

References

[1] World Health Organization, “Global status report on road safety 2018,” https://www.who.int, 2018.

[2] Ministry of Road Transport and Highways, “Road accidents in india 2022,” Government of India, Tech. Rep., 2023. [Online]. Available: https://morth.nic.in

[3] L. J. Miller, M. S. Salah, and R. W. Allen, “Development of a roll stability control model for a tractor trailer vehicle,” *SAE Int. J. Commer. Veh.*, no. 2009-01-0451, 2009.

[4] G. Morrison and D. Cebon, “Combined emergency braking and turning of articulated heavy vehicles,” *Veh. Syst. Dyn.*, vol. 55, no. 8, pp. 1089–1112, 2017.

[5] H. Patil, K. B. Devika, and S. C. Subramanian, “Direct yaw-moment control integrated with wheel slip regulation for heavy commercial road vehicles,” *IEEE Access*, vol. 10, pp. 116 284–116 300, 2022.

[6] X. Wang, W. Chen, J. Wu, and J. Wang, “Coordinated control of vehicle direct yaw moment and anti-lock braking systems under complex driving conditions,” *IEEE Access*, vol. 6, pp. 38 805–38 819, 2018.

[7] H. Patil, K. B. Devika, and S. C. Subramanian, “Integrated control of yaw moment and wheel slip for heavy commercial road vehicles,” in *Proc. Eur. Control Conf. (ECC)*, 2020, pp. 118–123.

[8] M. De Bernardis *et al.*, “On nonlinear model predictive direct yaw moment control with hitch angle measurement,” *Veh. Syst. Dyn.*, vol. 61, no. 3, pp. 445–473, 2023.

[9] L. Jin *et al.*, “A direct yaw moment control frame through model predictive control,” *Control Eng. Pract.*, 2024.

[10] Y. Cai *et al.*, “Hybrid physics and neural network model for lateral vehicle dynamics,” *Proc. Inst. Mech. Eng. D, J. Automob. Eng.*, 2024.

[11] J. Kontos *et al.*, “Prediction for future yaw rate values of vehicles using long short-term memory network,” *Sensors*, vol. 23, no. 12, p. 5670, 2023.

[12] H.-D. Arant, R. Siedersberger, S. C. Subramanian, and T. Kiencke, “Co-simulation of a heavy truck tire model and an electronic stability program,” in *Proc. FISITA World Automot. Congr.*, 2010.

[13] P. V. Gaurkar, K. Ramakrushnan, A. Challa, S. C. Subramanian, G. Vivekanandan, and S. Sivaram, “An anti-lock braking system algorithm using real-time wheel reference slip estimation and control,” *Proc. Inst. Mech. Eng. D, J. Automob. Eng.*, 2022.

[14] M. Mirzaeinejad and M. Mirzaei, “Optimization of nonlinear control strategy of vehicle braking dynamics based on prediction model of wheel slip,” *Transp. Res. C, Emerg. Technol.*, vol. 48, pp. 410–427, 2014.

[15] P. Li, W. Fu, W. Sun *et al.*, “Design and evaluation of cornering brake control for heavy vehicles,” *IET Intell. Transp. Syst.*, vol. 13, no. 10, pp. 1520–1528, 2019.

[16] R. Sukumaran, “Detection and prevention of untripped rollovers in heavy commercial road vehicles,” Ph.D. dissertation, Indian Institute of Technology Madras, 2024.

[17] H. B. Pacejka, *Tire and Vehicle Dynamics*, 3rd ed. Elsevier/Butterworth-Heinemann, 2012.

[18] N. Sridhar, K. B. Devika, S. C. Subramanian, G. Vivekanandan, and S. Sivaram, “Antilock brake algorithm for heavy commercial road vehicles with delay compensation and chattering mitigation,” *Veh. Syst. Dyn.*, vol. 59, no. 4, pp. 526–546, 2021.

[19] A. Challa, K. Ramakrushnan, P. V. Gaurkar, S. C. Subramanian, G. Vivekanandan, and S. Sivaram, “A 3-phase combined wheel slip and acceleration threshold algorithm for anti-lock braking in heavy commercial road vehicles,” *Veh. Syst. Dyn.*, 2021.

[20] National Highway Traffic Safety Administration, “Federal motor vehicle safety standard no. 136: Electronic stability control systems for heavy vehicles,” U.S. Dept. of Transportation, 49 CFR Part 571, 2015. [Online]. Available: https://www.nhtsa.gov